Thermochimica Acta 573 (2013) 25–31

Contents lists available at ScienceDirect

Thermochimica Acta

journal homepage: www.elsevier.com/locate/tca

Isothermal kinetics based on two-periods scheme for co-drying of biomass and lignite

H.M. Liu, M.Q. Chen*, Z.L. Han, B.A. Fu

School of Mechanical, Electronic and Control Engineering, Beijing Jiaotong University, Beijing 100044, China

ARTICLE INFO

Article history:
Received 10 May 2013
Received in revised form 27 August 2013
Accepted 28 August 2013
Available online 30 September 2013

Keywords:
Biomass
Lignite
Isothermal kinetics
Drying
Blend

ABSTRACT

Thermal gravimetric analysis (TGA) was applied to investigate the co-drying kinetics of biomass (Bermuda grass and red pine) with lignite. The drying rate of the lignite was much higher than that of the pure Bermuda grass and red pine. The drying of samples presented two distinctive falling rate periods. The activation energy of the pure Bermuda grass and red pine were higher than those of the grass/lignite and pine/lignite blends, respectively. In the first falling rate period, the dominant mechanism functions for the lignite, red pine and their blends were $1-(1-\alpha)^{1/3}$, and the functions were $1-(1-\alpha)^{0.5}$ in the Bermuda grass and its blends, while in the second falling rate period, the functions of the blends and their parent samples were $-\ln(1-\alpha)$. The drying kinetics of blends had no linear relation with blend ratios. The blending of the lignite with the grass or pine could improve the drying of the individuals.

© 2013 Elsevier B.V. All rights reserved.

1. Introduction

Lignite has high moisture content of 25–60%, which considerably limits its applications. For example, when low rank coals are burnt in boilers, about 7–10% of energy is used to evaporate the moisture in fuel [1]. It was calculated that the optimization of the drying process in future lignite power plants may lead to an efficiency increase of 4–6% [2–4]. The development of an efficient lignite drying process is a necessary step towards the implementation of the existing lignite-fuelled power plants [5,6]. Meanwhile, biomass is a renewable energy source that will provide environmental and economic benefits [7–10]. Due to the high volatile matter and moisture content, burning biomass alone cannot give very high energy output compared with coal combustion [11–13]. Co-firing biomass with coal in existing boilers to generate electricity has been proposed as a near-term, low-cost way to use biomass for reducing CO_2 emissions, furthermore, the existing coal-fuelled power plants can also be used with very few modifications [13–16]. However, biomasses with high inherent moisture content are similar to the lignite, and they should be dried before co-burning [17,18]. TG method has many advantages in drying, such as ease of operation, online recording of the drying process, and minimal material requirement. Chen et al. [19] obtained the drying characteristics of cotton stalk using the TG method by applying isothermal procedures. Tahmasebi et al. [20] gained the drying kinetics of an Indonesian low rank coal and found that the drying kinetics was best represented by two stages, the constant rate stage followed by the rate decay stage, and that the water removal rate was dependent mainly on drying temperature and coal sample size. Tahmasebi et al. [21] revealed the chemical structure changes of Chinese lignite during fluidized-bed drying in nitrogen and air. Kim et al. [22] examined the drying behaviour of low-rank Loy Yang coal in a fluidized bed dryer, and found that the drying rate increased with temperature and fluidization velocity increasing and relative humidity decreasing. Pakowski et al. [23] experimentally determined the effective diffusivity of water in brown coal in superheated steam at 200 °C and atmospheric pressure using slightly compressed pellets of cylindrical shape. Many studies mainly focused on drying of foods or grains below 100 °C in order to preserve and store [24–26]. For high moisture content matrixes, liquid diffusion is supposed to be the main mechanism of moisture transport in the first falling rate stage of drying while vapor diffusion is supposed to dominate in the second falling rate stage [27]. There were many studies primarily focused on co-combustion or pyrolysis of coal and biomass [28–32]. Many researchers have revealed some results on the drying kinetics of pure biomass and lignite, but little information is available to date on the potential impact of co-drying kinetics for biomass and lignite at medium temperatures, especially co-drying kinetics of lignite and Bermuda grass or red pine are not found in the literatures.

In the present work, thermal gravimetric analysis (TGA) was applied to investigate the isothermal co-drying kinetics of biomass (Bermuda grass and red pine) and lignite. The effects of temperatures, sample kinds and blending ratios on the kinetics parameters

---

* Corresponding author. Tel.: +86 10 51683423; fax: +86 10 82057443.
E-mail address: mqchen@bjtu.edu.cn (M.Q. Chen).

0040-6031/$ – see front matter © 2013 Elsevier B.V. All rights reserved.
http://dx.doi.org/10.1016/j.tca.2013.08.030

Nomenclature

a	weight loss rate
A	the pre-exponential or frequency factor (s^{-1})
DTG	drying rate (mg min^{-1})
E_a	apparent activation energy (J mol^{-1})
k	the reaction rate coefficient
M	mass fraction of sample
R	the universal gas constant [J/(mol K)]
t	time (s)
T	drying temperature (K)

Subscripts and superscripts

0	initial
∞	final

and mechanism were also investigated. This research will provide fundamental data for understanding the co-drying kinetics of biomass with lignite, and scientific reference for the design and improvement of the boiler.

2. Experimental facility and test samples

A thermogravimetric analyzer (TGA/SDTA851, Mettler Toledo) with a precision of 0.001 mg was used to conduct the drying experiments. Pulverized lignite, Bermuda grass and red pine particle were selected, and the biomass samples were crushed into 0.2–0. 6 mm in a high speed grinder, then, an electronic scale (FA1004, Heng Ping) with a precision of 0.1 mg was used to measure the mass of each sample. The mixtures were obtained from a platinum crucible in which the lignite/Bermuda grass and lignite/red pine blends were homogenized with biomass weight percentages of 20, 40, 60 and 80 wt.%, and the initial mass of each sample was maintained at 10 mg ± 0.5 mg. A crucible with the test samples was placed inside the drying chamber, and the drying processes were carried out under nitrogen with 40 mL/min flow. The thermal analyzer heated the sample from room temperature (20 °C) rapidly to the set temperature (50, 70, 90, 110, 130, 150 and 170 °C) and then stabilized. Proximate analyses of the parent samples were performed in the analyzer, detailed measuring method from the references [33,34]. The proximate analysis was listed in Table 1. The heating values in Table 1 were estimated by using the method in reference [35]. The ultimate analysis results for the parent samples [36–38] were also listed in Table 1.

3. Kinetics analytical method

The dependence of drying rate on temperature can be determined by the Arrhenius expression [39]:

$$\frac{d\alpha}{dt} = A \cdot e^{-\frac{E_a}{RT}} f(\alpha) \tag{1}$$

where E_a [J/mol] is the apparent activation energy required for the moisture migration; A [min^{-1}] the frequency factor; t [min] the time; R [J/(mol K)] the universal gas constant; and T [K] the absolute temperature; a the weight loss rate of samples at any time and it can be calculated using the following equation

$$a = \frac{m_0 - m}{m_0 - m_\infty} \tag{2}$$

where m is the weight of samples at any time, m_0 the initial weight of samples, and m_∞ the weight of samples at the end of the drying process, respectively. By the way, the mass fraction of samples, longitudinal coordinate in TG curves can be expressed as

$$M = \frac{m - m_\infty}{m_0 - m_\infty} = 1 - a \tag{3}$$

The integration function of Eq. (1) is given by:

$$g(\alpha) = \int \frac{d\alpha}{f(\alpha)} \tag{4}$$

Substituting of Eq. (1) into (4), and based on the isothermal kinetics, the integration function is described as follows:

$$g(\alpha) = kt + b \tag{5}$$

where k is the reaction rate coefficient, $g(\alpha)$ a function depending on the mechanism assumed for the reaction. Substituting each common mechanism function shown in Table 2 into Eq. (5), and then the function is obtained by using the double logarithm method based on Avrarni–Erofeev equation [40–42]:

$$1 - \alpha = e^{-kt^m} \tag{6}$$

Double logarithm form about Eq. (6) is written as:

$$\ln[-\ln(1-\alpha)] = m \ln t + \ln k \tag{7}$$

By plotting $\ln[-\ln(1-\alpha)]$ vs.ln t, the m value is obtained at certain drying temperature. The m value is compared with those for the different kinetic models in Table 2, then the only mechanism function is selected. Furthermore, k value is got by plotting $g(\alpha)$ vs. t.

The logarithm form of Arrhenius principle is set down [43]:

$$\ln k = -\frac{E_a}{RT} + \ln A \tag{8}$$

By plotting ln (k) vs. 1/T, E_a and A can be subsequently related to drying conditions.

4. Results and discussion

4.1. Thermogravimetric and differential thermogravimetric analysis

The TG and DTG curves of samples in different temperatures were obtained, but only partial results were presented due to the limited space. Figs. 1 and 2 illustrated the TG and DTG curves, respectively. The drying rate was equal to DTG value which was the variation of sample weight per unit time during the drying process.

From the figures, the drying rate of the lignite was much higher than that of the pure Bermuda grass and red pine at the same drying temperature, and those of the Bermuda grass/lignite and pine/lignite blends were between the lignite and Bermuda grass or red pine, respectively. The drying of the Bermuda grass and red pine presented thermal lag characters compared with that of the lignite. This could be due to much bound water (bound to the inner pores of raw materials) in biomass and much free water (bound to the particle surface and existing in pores of raw materials) in the lignite with strong water-absorbing. The drying rates of the pure Bermuda grass and grass/lignite blends were higher than those of the pure red pine and pine/lignite blends pure due to that the red pine was belong to woody biomass with dense structure, and low moisture contents as shown in Table 1. As illustrated in Fig. 2, drying of samples presented three distinct periods, initial period, first falling rate period and second falling rate period. The initial period was the beginning of drying, which drying rate depended on the external process parameters. The slope of the DTG curve increased in a short time and the drying rate reached its maximum value rapidly. In this period, evaporation occurred only from the

Table 1
Proximate and ultimate analyses of samples.

Samples	Proximate analyses (%)				Ultimate analyses (%)					HHV (kJ/kg)
	M_{ad}[a]	V_{ad}	FC_{ad}	A_{ad}	C_{ar}[b]	H_{ar}	N_{ar}	O_{ar}	S_{ar}	
Lignite	9.73	30.96	47.39	11.92	56.72	3.61	0.71	15.98	9.73	21.67
Bermuda grass	7.26	67.82	11.52	13.4	46.80	6.12	0.91	41.66	0.25	17.91
Red pine	5.35	64.66	21.65	8.14	49.30	6.30	0.01	44.10	<0.01	17.67

[a] ad refers to moisture content, volatile substance content, fixed carbon content and ash content in sample corresponding to air dried basis.
[b] ar is the abbreviation of ‘as received basis’.

Table 2
The common mechanism functions for solid reactions.

Functions	$g(\alpha)$	m	Functions	$g(\alpha)$	m
$D_1(\alpha)$	$\alpha^2 = kt$	0.62	$R_2(\alpha)$	$1-(1-\alpha)^{1/2} = kt$	1.11
$D_2(\alpha)$	$(1-\alpha)\ln(1-\alpha)+\alpha = kt$	0.57	$R_3(\alpha)$	$1-(1-\alpha)^{1/3} = kt$	1.07
$D_3(\alpha)$	$[1-(1-\alpha)^{1/3}]^2 = kt$	0.54	$A_2(\alpha)$	$[-\ln(1-\alpha)]^{1/2} = kt$	2.00
$F_1(\alpha)$	$-\ln(1-\alpha) = kt$	1.00	$A_3(\alpha)$	$[-\ln(1-\alpha)]^{1/3} = kt$	3.00

surface of the sample and since heat transfer promoted the evaporation, the radius of the liquid/vapor interface over the exterior surface decreased continuously. Meanwhile, the rapid heating may have caused considerable expansion (puffing) of the small samples, resulting in rapid evaporation and vapor diffusion. This period existed for a very short period of time, approximately 0.5–1.5 min depending on the drying temperature and blending ratio used.The maximum drying rate point was taken as a turning point (the first critical point) of the initial period and the falling rate period [17,43]. The first falling rate period, just beyond the first critical point, the liquid/vapor interface had entered the pores and the liquid receded into the pores. During this period, the rate of evaporation of surface of outside decreased rapidly due to the increasing resistance of interface moving towards internal and the decreasing moisture content, the drying rate clearly decreased. During the transition of the first falling rate period to second falling rate period, there was possibly a change from porous tissue structure to an increasingly non-permeable structure. The shrinkage might have caused a denser and tougher structure which might increase the resistance to internal moisture movement, therefore the drying rates in the

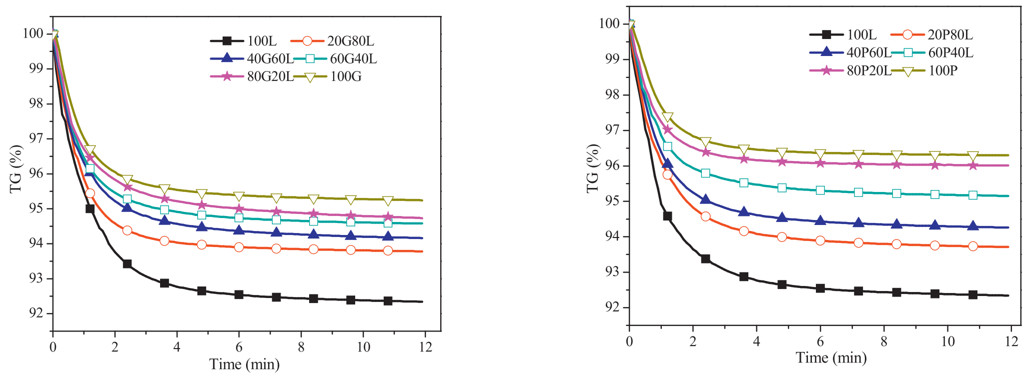

(a) Bermuda grass / lignite at 130℃ drying temperature (b) Red pine / lignite at 130℃ drying temperature

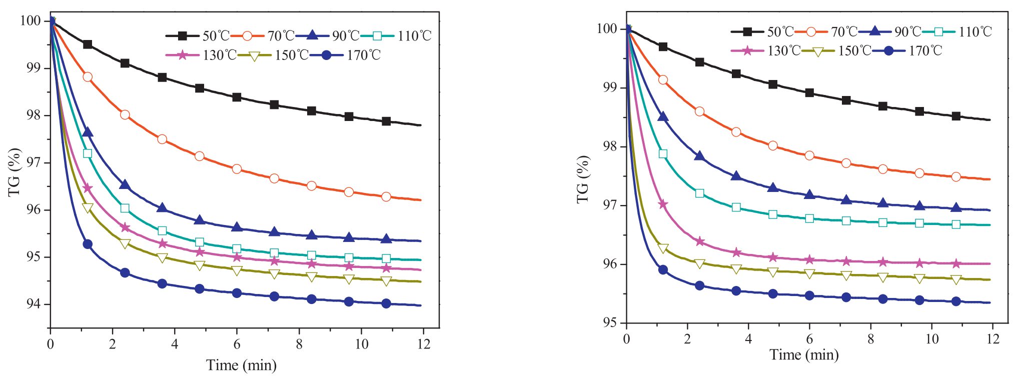

(c) 80G20L[a] (d) 80P20L[b]

Fig. 1. TG curves of biomass/lignite.

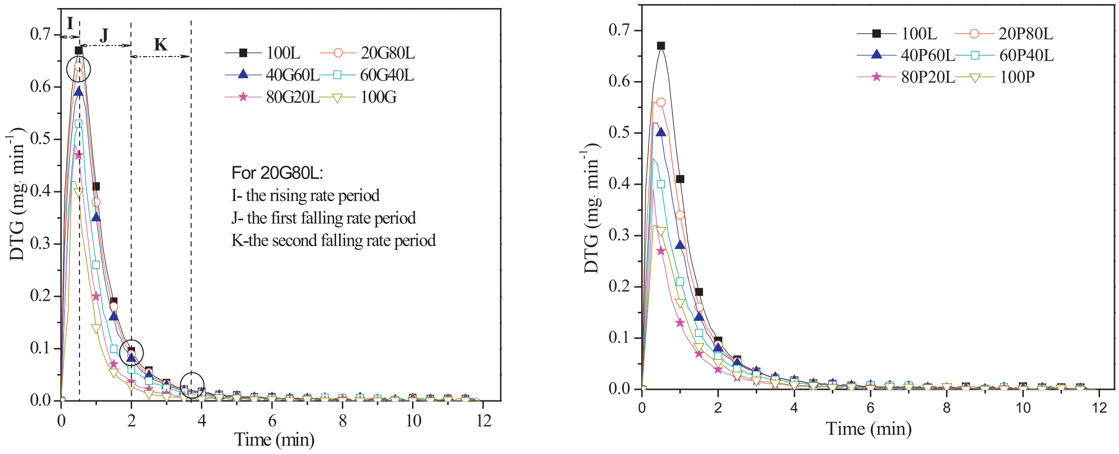

(a) Bermuda grass / lignite at 130℃ drying temperature (b) Red pine / lignite at 130℃ drying temperature

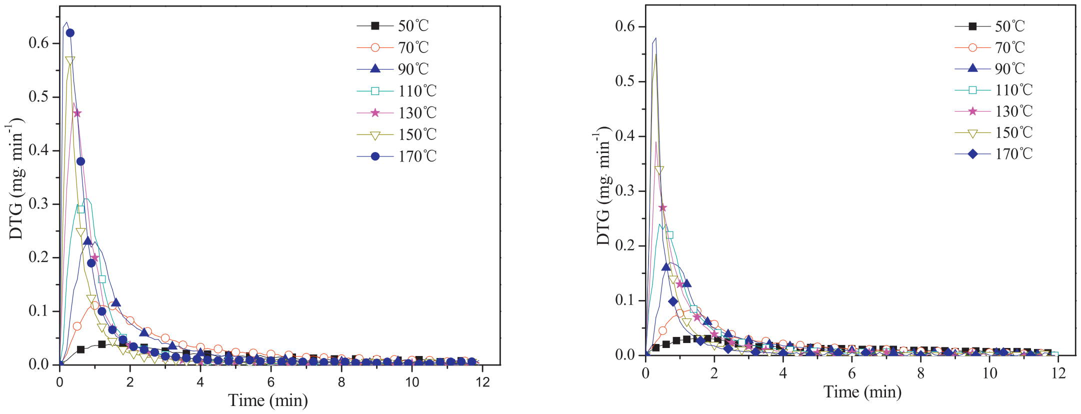

(c) 80G20L (d) 80P20L

Fig. 2. DTG curves of biomass/lignite.

second falling rate period decreased slowly than the first falling rate period. Casehardening was another possible reason for low drying rate in the 2nd falling rate period.

The drying rate of the blends increased with increasing the drying temperature because of the reinforce of moisture migration, which resulted from the enhancement of driving force on heat transfer in the samples. For example, the maximums of the drying rates at 170 °C were about 16 times and 15 times higher than those at 50 °Cfor the 80G/20L blend and 80P/20L blend, respectively.

4.2. Kinetic analysis

In order to accurately reveal the co-drying behaviour of blends in whole falling rate stage, the drying kinetics of the first falling rate period and the second falling rate period were distinguished. Fig. 3 presented the linear fitting by plotting $\ln[-\ln(1-\alpha)] \sim \ln t$ for the 80G20L blend in the first falling rate period at 130 °C. The m value was 1.091, which was close to 1.11, so $R_2(\alpha)$ was taken as a suitable mechanism function. The k value was 0.394 min^{-1}, which was obtained by plotting the $g(\alpha)$ vs. t, as shown in Fig. 4. The method might also be applied to other drying temperatures, and other period, and other samples.

The activation energy and the frequency factor of blend were obtained by plotting $\ln(k)$ vs. $1/T$ in the first falling period as shown in Fig. 5, from which E_a and A values were predicted, 15.08 kJ/mol and $10^{1.53}$ min^{-1}, respectively. The method might be also applied to other period and other samples. The results were presented in Table 3.

The activation energy of the lignite was higher than those of the pure Bermuda grass, red pine and blends. The activation energy of the pure Bermuda grass and red pine were higher than those of the grass/lignite and pine/lignite blends, respectively, indicating that the blending of the lignite with the Bermuda grass or red

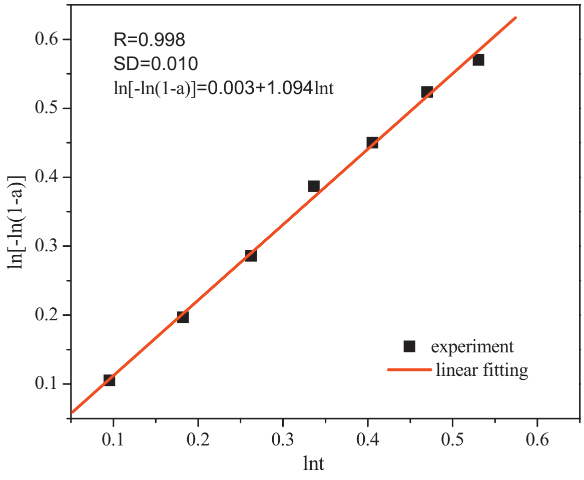

Fig. 3. Linear fitting of drying of the 80G20L blend at 130 °C by lnln method.

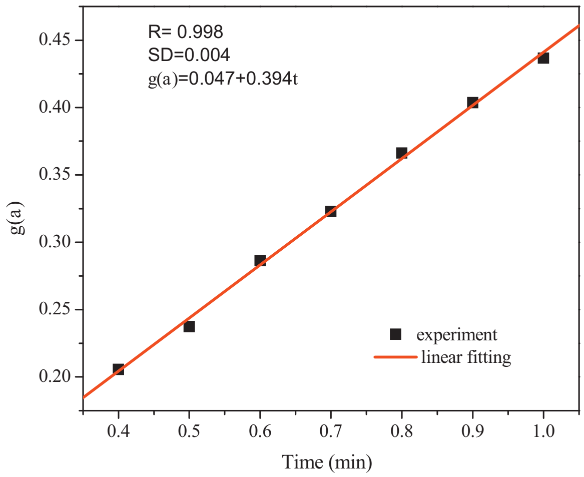

Fig. 4. Linear fitting between G(α) vs. t for the 80G20L blend at 130 °C.

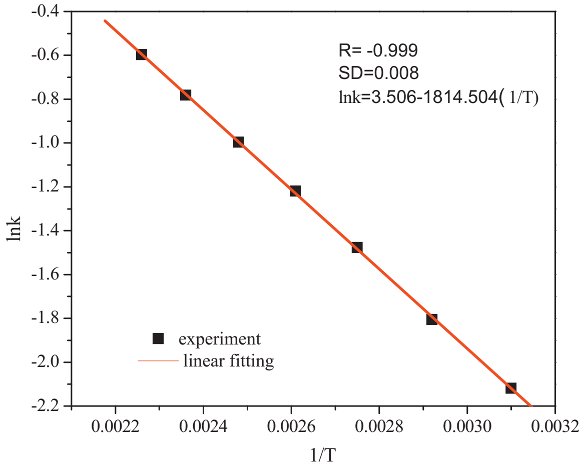

Fig. 5. Arrhenius-type relationship between ln (k) vs. 1/T for the 80G20L blend in the first falling period.

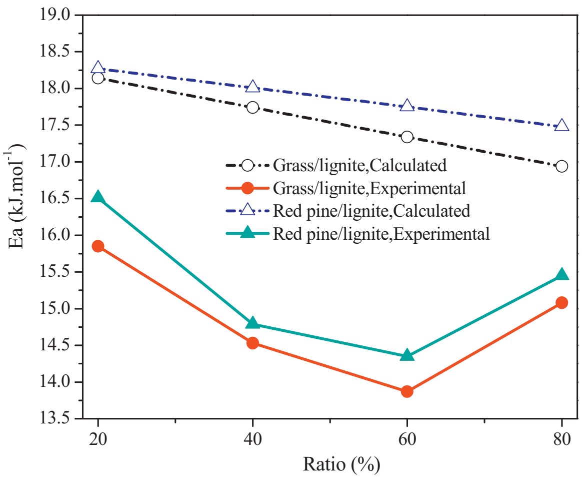

(a) 1stfalling rate period

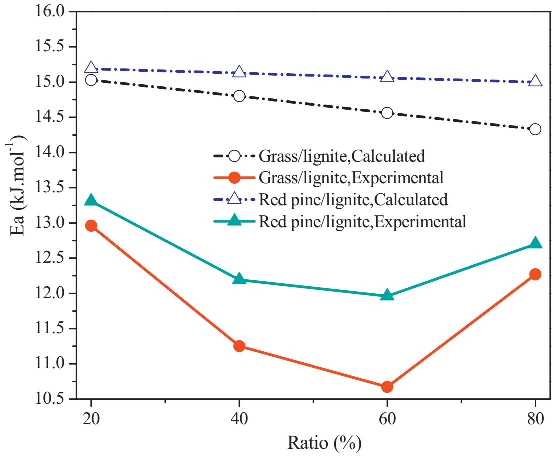

(b) 2ndfalling rate period

Fig. 6. Comparison between calculated activation energy and real values.

pine could improve the drying of the lignite and Bermuda grass or red pine. The grass/lignite and pine/lignite blends can be dried under lower temperature than their parent samples. The activation energy of samples in the first falling rate period was much higher than that in the second falling rate period, which was attributed to the reducing of bound water in the sample. In order to find out whether interactions between the components of the blends occurred, the activation energy of the blends calculated by using the ratio of samples in the first falling rate period and the second falling rate period as shown in Fig. 6. The drying kinetics characteristics of the blends had no linear relation with blend ratios due to interaction between the lignite and Bermuda grass or red pine, and the real values were much lower than the calculated values, indicating that there were synergistic interactions between the parent samples during the co-drying of the lignite and Bermuda grass or red pine.

Table 3
Kinetic parameters and mechanism functions of the drying of samples.

Samples	1st falling rate					2nd falling rate				
	E_a (kJ/mol)	A (min^{-1})	$g(\alpha)$	R	SD	E_a (kJ/mol)	A (min^{-1})	$g(\alpha)$	R	SD
100L	18.53	$10^{1.82}$	R3	−0.999	0.006	15.26	$10^{1.74}$	F1	−0.998	0.006
20G80L	15.85	$10^{1.61}$	R2	−0.994	0.011	12.96	$10^{1.49}$	F1	−0.998	0.003
40G60L	14.53	$10^{1.52}$	R2	−0.995	0.008	11.25	$10^{1.28}$	F1	−0.997	0.005
60G40L	13.87	$10^{1.46}$	R2	−0.997	0.004	10.67	$10^{1.21}$	F1	−0.997	0.004
80G20L	15.08	$10^{1.53}$	R2	−0.999	0.008	12.27	$10^{1.33}$	F1	−0.998	0.004
100G	16.54	$10^{1.74}$	R2	−0.999	0.003	14.1	$10^{1.67}$	F1	−0.997	0.006
20P80L	16.51	$10^{1.61}$	R3	−0.997	0.005	13.31	$10^{1.53}$	F1	−0.996	0.008
40P60L	14.79	$10^{1.36}$	R3	−0.995	0.004	12.19	$10^{1.36}$	F1	−0.997	0.006
60P40L	14.35	$10^{1.30}$	R3	−0.999	0.006	11.96	$10^{1.28}$	F1	−0.996	0.007
80P20L	15.45	$10^{1.53}$	R3	−0.996	0.008	12.7	$10^{1.45}$	F1	−0.999	0.008
100P	17.22	$10^{1.79}$	R3	−0.999	0.006	14.93	$10^{1.68}$	F1	−0.997	0.005

Moreover, in the first falling rate period, the mechanism functions of the drying for the lignite, pure red pine and their blends were $1-(1-\alpha)^{1/3}$, which was controlled by the phase boundary reaction and spherical symmetry. The rate of water loss is dominated by the rate of an interface advance, which generated between reactant and product phase. The formula is also known as the contracting volume (cube or sphere) equation, which can describe rate variation of interface advance in different directions. The mechanism functions of the Bermuda grass and its blends with the lignite were $1-(1-\alpha)^{0.5}$, which was controlled by the phase boundary reaction and cylindrical symmetry. This rate equation derived from a reaction readily initiated at all surfaces of a cylinder or column-shaped prism of reactant, or the interface moving inwards from the edges of a disc or plate-like particle. In the second falling rate period, the functions of the grass/lignite blends, pine/lignite blends and their parent samples were $-\ln(1-\alpha)$, which was controlled by the random nuclear producing and growing process. Nucleation is often considered as a series of chemical changes across reactant surfaces, which initiated by an advancing energetic wave occurring randomly at the reactant/product interface. Growth is the maintained reaction within the interface between the reactant and product phases.

5. Conclusions

The drying rate of the lignite was much higher than those of the pure Bermuda grass and red pine, and those of the grass/lignite and pine/lignite blends were in between those of the lignite and Bermuda grass or red pine. The drying of the Bermuda grass and red pine presented thermal lag characters compared with that of the lignite. The drying rate of blend increased with increasing the drying temperature. The drying of samples presented two obvious falling rate periods. In the first falling rate period, the mechanism function of drying for the lignite, pure red pine and their blends were fitted to $1-(1-\alpha)^{1/3}$, and the functions of the Bermuda grass and its blends with the lignite were fitted to $1-(1-\alpha)^{0.5}$, while in the second falling rate period, the functions of the grass/lignite blends, pine/lignite blends and their parent samples were fitted to $-\ln(1-\alpha)$. There were synergistic interactions between the parent samples during the co-drying of the lignite and Bermuda grass or red pine.

Acknowledgment

This work was supported by the National Natural Science Foundation of China under No 51376017.

References

[1] M. Karthikeyan, W. Zhonghua, A.S. Mujumdar, Low-rank coal drying technologies – current status and new developments, Drying Technology 27 (2009) 403–415.

[2] M. Agraniotis, P. Grammelis, C. Papapavlou, E. Kakaras, Experimental investigation on the combustion behaviour of pre-dried Greek lignite, Fuel Processing Technology 90 (2009) 1071–1079.

[3] J. Bugge, S. Kjær, R. Blum, High-efficiency coal-fired power plants development and perspectives, Energy 31 (2006) 1437–1445.

[4] M. Aziz, Y. Kansha, A. Tsutsumi, Self-heat recuperative fluidized bed drying of brown coal, Chemical Engineering and Processing: Process Intensification 50 (2011) 944–951.

[5] C. Bergins, J. Hulston, K. Strauss, A.L. Chaffee, Mechanical/thermal dewatering of lignite. Part 3: Physical properties and pore structure of MTE product coals, Fuel 86 (2007) 3–16.

[6] Y. Fei, Y. Artanto, L. Giroux, M. Marshall, W.R. Jackson, J.A. MacPhee, J.P. Charland, A.L. Chaffee, D.J. Allardice, Comparison of some physico-chemical properties of Victorian lignite dewatered under non-evaporative conditions, Fuel 85 (2006) 1987–1991.

[7] D. Vamvuka, S. Sfakiotakis, Combustion behaviour of biomass fuels and their blends with lignite, Thermochimica Acta 526 (2011) 192–199.

[8] M.M. Roy, A. Dutta, K. Corscadden, P. Havard, L. Dickie, Review of biosolids management options and co-incineration of a biosolid-derived fuel, Waste Management 31 (2011) 2228–2235.

[9] T. Abbasi, S.A. Abbasi, Biomass energy and the environmental impacts associated with its production and utilization, Renewable and Sustainable Energy Reviews 14 (2010) 919–937.

[10] R. Saidur, E.A. Abdelaziz, A. Demirbas, M.S. Hossain, S. Mekhilef, A review on biomass as a fuel for boilers, Renewable and Sustainable Energy Reviews 15 (2011) 2262–2289.

[11] M.V. Gil, D. Casal, C. Pevida, J.J. Pis, F. Rubiera, Thermal behaviour and kinetics of coal/biomass blends during co-combustion, Bioresource Technology 101 (2010) 5601–5608.

[12] L.I. Darvell, J.M. Jones, B. Gudka, X.C. Baxter, A. Saddawi, A. Williams, A. Malmgren, Combustion properties of some power station biomass fuels, Fuel 89 (2010) 2881–2890.

[13] M. Aho, A. Gil, R. Taipale, P. Vainikka, H. Vesala, A pilot-scale fireside deposit study of co-firing Cynara with two coals in a fluidised bed, Fuel 87 (2008) 58–69.

[14] J. Hansson, G. Berndes, F. Johnsson, J. Kjärstad, Co-firing biomass with coal for electricity generation – an assessment of the potential in EU27, Energy Policy 37 (2009) 1444–1455.

[15] M. Otero, M.E. Sánchez, X. Gómez, Co-firing of coal and manure biomass: a TG-MS approach, Bioresource Technology 102 (2011) 8304–8309.

[16] M.L. Kubacki, A.B. Ross, J.M. Jones, A. Williams, Small-scale co-utilisation of coal and biomass, Fuel 101 (2012) 84–89.

[17] M. Phanphanich, S. Mani, Impact of torrefaction on the grindability and fuel characteristics of forest biomass, Bioresource Technology 102 (2011) 1246–1253.

[18] P. Rousset, C. Aguiar, N. Labbé, J.M. Commandré, Enhancing the combustible properties of bamboo by torrefaction, Bioresource Technology 102 (2011) 8225–8231.

[19] D. Chen, Y. Zheng, X. Zhu, Determination of effective moisture diffusivity and drying kinetics for poplar sawdust by thermogravimetric analysis under isothermal condition, Bioresource Technology 107 (2012) 451–455.

[20] A. Tahmasebi, J. Yu, X. Li, C. Meesri, Experimental study on microwave drying of Chinese and Indonesian low-rank coals, Fuel Processing Technology 92 (2011) 1821–1829.

[21] A. Tahmasebi, J. Yu, Y. Han, X. Li, A study of chemical structure changes of Chinese lignite during fluidized-bed drying in nitrogen and air, Fuel Processing Technology 101 (2012) 85–93.

[22] H.S. Kim, Y. Matsushita, M. Oomori, T. Harada, J. Miyawaki, S.H. Yoon, I. Mochida, Fluidized bed drying of Loy Yang brown coal with variation of temperature, relative humidity, fluidization velocity and formulation of its drying rate, Fuel 105 (2013) 415–424.

[23] Z. Pakowski, R. Adamski, S. Kwapisz, Effective diffusivity of moisture in low rank coal during superheated steam drying at atmospheric pressure, Chemical and Process Engineering – Inzynieria Chemiczna i Procesowa 33 (2012) 43–51.

[24] A. Kaleta, K. Górnicki, Some remarks on evaluation of drying models of red beet particles, Energy Conversion and Management 51 (2010) 2967–2978.

[25] M. Zielinska, M. Markowski, Air drying characteristics and moisture diffusivity of carrots, Chemical Engineering and Processing: Process Intensification 49 (2010) 212–218.

[26] O. Dixit, K. Treppe, A. Khaidurova, N. Mollekopf, Experimental investigation and theoretical modelling of absolute convective drying of starch, Journal of Food Engineering 111 (2012) 14–20.

[27] L. Hassini, S. Azzouz, R. Peczalski, A. Belghith, Estimation of potato moisture diffusivity from convective drying kinetics with correction for shrinkage, Journal of Food Engineering 79 (2007) 47–56.

[28] Z. Liu, A. Quek, S. Kent Hoekman, M.P. Srinivasan, R. Balasubramanian, Thermogravimetric investigation of hydrochar-lignite co-combustion, Bioresource Technology 123 (2012) 646–652.

[29] K. Zhang, Y. Cao, W.P. Pan, Co-combustion characteristics and blending optimization of tobacco stem and high-sulfur bituminous coal based on thermogravimetric and mass spectrometry analyses, Bioresource Technology 131 (2013) 325–332.

[30] G. Di Nola, W. de Jong, H. Spliethoff, TG-FTIR characterization of coal and biomass single fuels and blends under slow heating rate conditions: Partitioning of the fuel-bound nitrogen, Fuel Processing Technology 91 (2010) 103–115.

[31] P.C.W. Kwong, C.Y.H. Chao, J.H. Wang, C.W. Cheung, G. Kendall, Co-combustion performance of coal with rice husks and bamboo, Atmospheric Environment 41 (2007) 7462–7472.

[32] C. Wang, Y. Wu, Q. Liu, H. Yang, F. Wang, Analysis of the behaviour of pollutant gas emissions during wheat straw/coal cofiring by TG-FTIR, Fuel Processing Technology 92 (2011) 1037–1041.

[33] M. Varol, A.T. Atimtay, B. Bay, H. Olgun, Investigation of co-combustion characteristics of low quality lignite coals and biomass with thermogravimetric analysis, Thermochimica Acta 510 (2010) 195–201.

[34] M.C. Mayoral, M.T. Izquierdo, J.M. Andrés, B. Rubio, Different approaches to proximate analysis by thermogravimetry analysis, Thermochimica Acta 370 (2001) 91–97.

[35] J. Parikh, S.A. Channiwala, G.K. Ghosal, A correlation for calculating HHV from proximate analysis of solid fuels, Fuel 84 (2005) 487–494.

[36] A.M. Rizzo, M. Prussi, L. Bettucci, I.M. Libelli, D. Chiaramonti, Characterization of microalga Chlorella as a fuel and its thermogravimetric behavior, Applied Energy 102 (2013) 24–31.

[37] J. Wang, W. Fan, Y. Li, M. Xiao, K. Wang, P. Ren, The effect of air staged combustion on NO_x emissions in dried lignite combustion, Energy 37 (2012) 725–736.

[38] A.A. Boateng, W.F. Anderson, J.G. Phillips, Bermudagrass for biofuels: effect of two genotypes on pyrolysis product yield, Energy & Fuels 21 (2007) 1183–1187.

[39] S. Biswas, P. Mohanty, D.K. Sharma, Studies on synergism in the cracking and co-cracking of Jatropha oil, vacuum residue and high density polyethylene: Kinetic analysis, Fuel Processing Technology 106 (2013) 673–683.

[40] J.M. Criado, On the theoretical basis of the hancock and sharp “ln.ln method” of kinetic analysis of isothermal data, Thermochimica Acta 39 (1980) 361–362.

[41] M. Erceg, T. Kovačić, I. Klarić, Poly(3-hydroxybutyrate) nanocomposites: Isothermal degradation and kinetic analysis, Thermochimica Acta 485 (2009) 26–32.

[42] J.M. Criado, A. Ortega, C. Real, E. Torres De Torres, Re-examination of the kinetics of the thermal dehydroxylation of kaolinite, Clay Minerals 19 (1984) 653–661.

[43] M.Q. Chen, Y.X. Chen, L. Jia, Y.G. Zhang, Q.H. Li, A.H. Meng, Kinetic analysis on the drying of high moisture MSW, Heat Transfer – Asian Research 38 (2009) 216–222.